Non-local fatigue criterion based on standard deviation for notches and defects in Ti-6Al-4V

Natan Bodlet, Rémi Amargier, Yves Nadot

Non-local fatigue criterion based on standard deviation for notches and defects in Ti-6Al-4V.

N. Bodlet (1,2), R. Amargier (2) and Y.Nadot (1)

(1) Institut Pprime, ISAE-ENSMA, CNRS, Université de Poitiers, France

(2) Airbus Operation SAS, Toulouse, France

Abstract

The aim of this study is to propose a non local multiaxial fatigue criterion in order to assess the fatigue limit of stress concentrator such as notches or defects in Ti-6Al-4V. This criterion is based on the standard deviation of the stresses integrated over a given volume around the hot spot point. Four parameters are necessary to identify the criterion. The criterion is first validated on notched samples based on literature results and shows very good results. A set of experimental tests is conducted on natural and artificial defects including clustering defects and demonstrates the flexibility and accuracy of the criterion.

Nomenclature

$\sqrt{J_{2,a}}$	= Amplitude of the second invariant of the deviatoric stress tensor
$\sqrt{area}$	= Murakami's parameter
α_{cr} , β_{cr}	= Crossland parameters
γ	= Weight given to the stress field variation (standard deviation)
$J_{1,max}$	= Maximum value over a period of the first invariant stress tensor
$sd(J_{1,max})_r$	= Standard deviation in the integration domain
ρ	= Root radius
σ_a	= Fatigue limit amplitude
σ_{ave}	= Stress average volume approach
σ_{cr}	= Crossland criterion
$\sigma_{cr,max}$	= Crossland value at the hot point
σ_{grad}	= Linear gradient approach
$\sigma_{grad\ nl}$	= Non-linear gradient approach
σ_{sd}	= New criterion based on the standard deviation
a_{grad}	= Linear gradient approach parameter
d	= Net section diameter
d1, d2	= Mill diameters
D	= Specimen diameter
r	= Radius of integration
r^2	= Coefficient of correlation
R	= Loading ratio
n	= Non-linear gradient approach parameter

Keywords: Fatigue ; Multiaxial criterion ; Standard deviation ; Gradient effect ; Ti-6Al-4V

Introduction

This paper deals with the consideration of stress heterogeneity over an integration domain and leads to the formulation of a multiaxial and non-local fatigue criterion. The use of a local stresses value often doesn't predict the fatigue limit of a component with a stress concentrator, it is most of the time conservative. For 20 years, the fatigue design under strong gradient has been of major interest. Among the large literature we have selected five methods that aim to study this problem: critical point, line and surface distance theory (1999) (1); gradient approach (1996) (2)(3); strongly stressed volume theory V90% (1960) (4); integral approach (2015) (5); probabilistic approach (2013) (6). Recent conclusions will be presented to address the question: "*What is the most relevant indicator to describe the effect of stress heterogeneity with a stress concentrator on fatigue strength*?". In a study conducted by Vincent (7), which may be a source of inspiration, the author seeks to describe, by a multiaxial fatigue criterion, the continuity between crack initiation in smooth sample and initiation on defect. For this, it realizes an aggregate of anisotropic behaviours composed of elastic grains (Fig. 1a), where a defect is introduced in the centre of a small volume. From a certain size (critical defect size), the defect will be the initiation site and a reduction on the fatigue limit is observed. For comparison purposes, an experimental reference is carried out by tests on pure Armco iron specimens in the presence of artificial defects. The Kitagawa diagram is generally composed of a first zone where the defects are too small to induce a reduction on the fatigue limit, the initiations take place in the microstructure or on the defect but without effect on the fatigue limit. In the study (7), experimental and numerical Kitagawa diagrams are compared (Fig. 1b). Vincent shows that the transition from microstructure initiation to defect initiation can be correlated with experiment and the critical defect size can be evaluated numerically. On the other hand, for larger defect sizes, the evaluation of the fatigue criterion had to be modified: "the modification of the mesoscopic criterion by taking into account intragranular heterogeneities (via the standard deviation per grain of the mechanical quantities) makes the criterion less conservative (by straightening the slope of the simulated Kitagawa diagram) while maintaining a good description for small defects"(7). Vincent proposes the innovative idea of subtracting the standard deviation of the equivalent stresses over one grain from the value of the average equivalent stress of the grain (Eq. (1)). Thus, it considers by an indicator of dispersion, intragranular heterogeneity. This is done by adding a parameter γ.

$$\sigma_{grain} = \sigma_{cr\ average\ grain} - \gamma . \sigma_{cr\ standard\ deviation\ \ grain} \qquad (1)$$

In 2021, Heyraud (8) uses the integral approach to calculate the High Cycle Fatigue of welded steel structures S355MC, he scans a wide range of elementary structures types represented in Fig. 1c. He considers only the average of the equivalent Dang Van stresses present in an integration sphere (Fig. 1d). His final intuition is as follows: "*One way to better understand gradient effects would be to consider the variance of the stress field within the integration domain instead of taking into account only the mean*" (8).

First, we will detail the multiaxial and non-local fatigue criteria that we propose, then we will develop the identification strategy. Later, we will apply to notches and defects. The notched fatigue results come from a database present in the literature (9). The natural porosities of our study result from the

electron beam welding process and are present in a welded joint. The artificial defects we have studied are machined on the side of welded joint. Finally, we discuss the criterion performance as well as ways to improve the predictive ability.

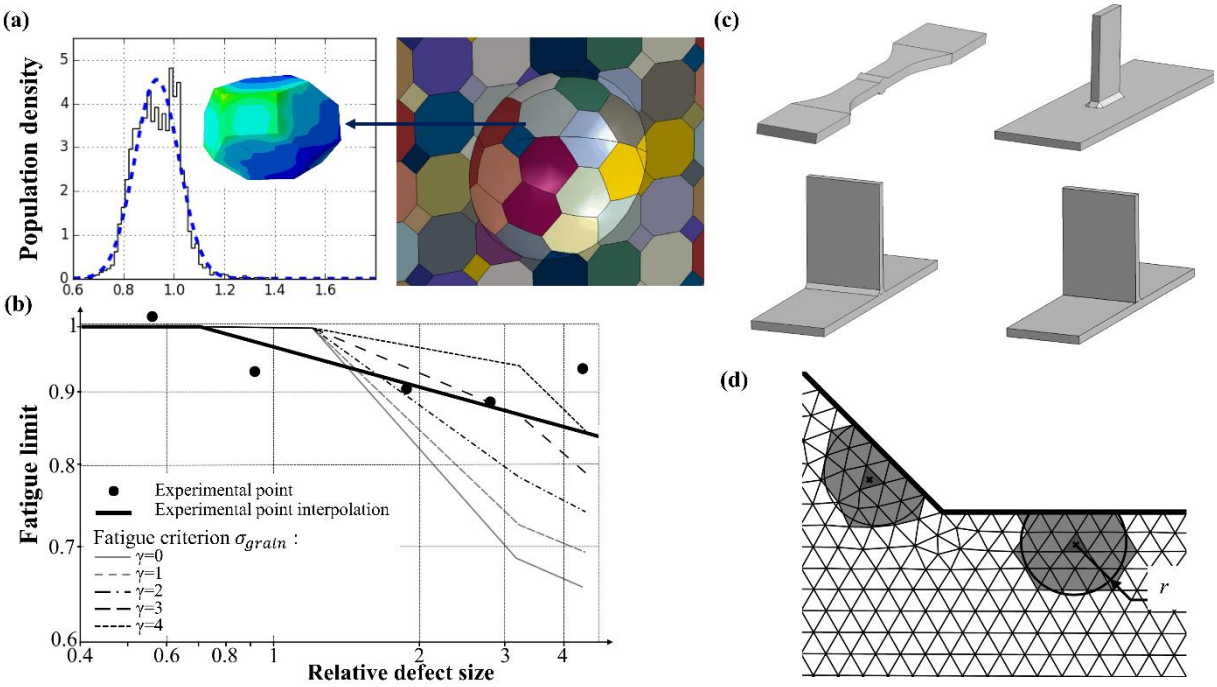

Fig. 1 : (a) Numerical distribution of Crossland equivalent stress in aggregate grain (7) ; (b) Kitagawa diagram: experimental/numerical comparison, fatigue criterion (Eq. (1))(7) ; (c) Welded structures tested by Heyraud (8) ; (d) Integration sphere in the connection area (8).

Non-local multiaxial fatigue criterion based on standard deviation

The consideration of the stress heterogeneity by using standard deviation in the integration domain have never been studied to our knowledge, it appears as a promising track. The new criterion will have two parts: a local value of the stresses and a value to consider the stresses variation in the integration domain. The integration domain will be a circle (2D) or a sphere (3D). The purpose of the local value is to locate the initiation site and the standard deviation aims at quantifying the stress heterogeneity effect. The criterion will now be justified and discussed.

The areas with the highest local stresses are most of the time the initiation sites when considering notches or defects. Therefore, a local value has the ability to identify the initiation location, which is why it is included in the new criterion. However, its ability to predict fatigue by only local value is too conservative. To understand the stress gradient, the study of the literature highlights the importance of the stress heterogeneity in the integration domain. The choice of the morphology of the integration domain is a circle or a sphere, but this is totally arbitrary. The local stress value chosen is the Crossland criterion, because of the multi-axiality related to the presence of geometric singularities. It is based on two invariants of the stress tensor. The first is the square root of the amplitude of the second invariant of the deviatoric stress tensor denoted $\sqrt{J_{2,a}}$. The second is the maximum value over a period of the first invariant stress tensor, denoted $J_{1,max}$. Crossland proposes to relate linearly $\sqrt{J_{2,a}}$ to

$J_{1,max}$ by a coefficient α_{cr} applied to $J_{1,max}$, compared to a threshold denoted β_{cr} (Eq. (2)).The α_{cr} and β_{cr}

$$\sigma_{cr} = \sqrt{J_{2,a}} + \alpha_{cr}.J_{1,max} \leq \beta_{cr} \quad (2)$$

coefficients are two parameters experimentally identified (10).

In 1996, Papadopoulos and his co-author (2) experimentally found, for alternating torsion tests, that the fatigue limit depends directly on the diameter of the specimen. After distinguishing between the gradient effect and the pure size effect, they propose to integrate the stress gradient effect by a weight function only on the hydrostatic part of the Crossland criterion. In order to consider the stress gradient, Papadopoulos and his co-author invite us to use the gradient of $J_{1,max}$. Thus, to evaluate the standard deviation $sd(J_{1,max})_r$ the series considered is the one of the integration domain. The indicator most commonly used to quantify the dispersion of a statistical series is the standard deviation. It should be noted that this indicator is homogeneous throughout the elements of the series. To compare standard deviations with each other, it is important to check four rules: series must not have an outlier; the averages of the series must be relatively close; the distribution is unimodal; the distribution is symmetric. In our study, the first three rules are generally fulfilled but the fourth could be problematic, indeed, the stress distribution is dependent on the overall geometry: we will discuss this throughout this paper.

We have highlighted by the experiments of our study, for a fixed radius of integration denoted *r*, the existence of an empirical linear relationship between $\sigma_{cr,max}$, the local Crossland value at the hot point, and $sd(J_{1,max})_r$ translated into equation and thus forming a new criterion denoted σ_{sd} (Eq. (3)). Two parameters will have to be identified on the "non-local" part: the size of the integration domain, a radius denoted *r*, and the weight given to the stress field variation (standard deviation), denoted γ (Fig. 2).

$$\sigma_{sd} = \sigma_{cr,max} - \gamma.sd(J_{1,max})_r \leq \beta_{cr} \quad (3)$$

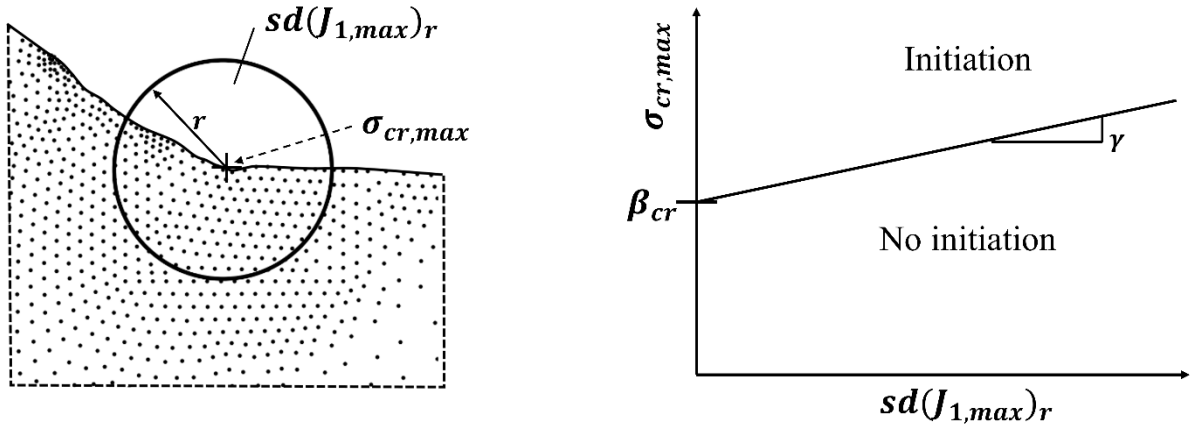

Fig. 2 : Multiaxial and non-local fatigue criterion σ_{sd}.

The identification strategy of Eq. (3) consists in identifying all the parameters, i.e. α_{cr}, β_{cr}, r and γ. The parameter α_{cr} is obtained thanks to two fatigue limits at different load ratios. The non-local parameters r and γ are obtained on a database with the most "morphologies" for the same type of concentrator. A concentrator such as notches or defects locally modifies the surface roughness, microstructure and residual stresses according to its type. Its type depends of its manufacturing process, such as machining speed or speed displacement for cutting… Using the database with the most morphologies obtains the most reliable non-local parameter. We assume that these parameters are independent of the type of stress concentrator, and therefore applicable to all types of stress concentrator. In a second step, β_{cr} is identified for each type of concentrator, so it carries the information related to the surface integrity of the concentrator.

Application to notches

In order to evaluate the criterion, we have compared to existing methods. We relied on a fatigue database of notched Ti-6Al-4V specimens (9) allowing us to test a wide range of geometries and load ratios (Table 1). The fatigue approaches to which we compare our criterion are: $\sigma_{cr,max}$, σ_{grad}, $\sigma_{grad\ nl}$ and σ_{ave}, detailed below:

- $\sigma_{cr,\ max}$: Maximum local Crossland stress

In order to check the necessity of applying non local approaches, the local maximum Crossland stress is included in the comparison.

- σ_{grad} : Linear gradient approach

The gradient approach was applied to capture the effect of stress gradient, it consists of adding a weight function to the local value (Eq. (4)) (11). This function is the multiplication of a parameter denoted a_{grad} and the stress gradient itself. The stress gradient can be approximated by Eq. (5) with ρ the notch root radius, $\sigma_{cr,max}$ the local Crossland value at the hot point and $\sigma_{cr}(\infty)$ the local Crossland value 'fare from the notch' following the direction of the strongest gradient. The use of this criterion implies knowledge of the direction of the strongest gradient, which is easily obtained for notched cylindrical specimens, because it is located on an axis of symmetry. Gradient approaches are most of the time based on the same general equation. The definition of the gradient can be adapted depending on the physical problem.

$$\sigma_{grad} = \sigma_{cr,max} - a_{grad}.grad(\sigma_{cr}) < \beta_{cr} \quad (4)$$

$$grad(\sigma_{cr}) = \frac{\sigma_{cr,max} - \sigma_{cr}(\infty)}{\rho} \quad (5)$$

- $\sigma_{grad\ nl}$: Non-linear gradient approach

In order to give saturation to the gradient effect, a parameter "n" can be subscripted by it, so the effect of the gradient is no longer linear (Eq. (6)). This non-linear criterion is commonly used in the literature as for example by Papadopoulos (2).

$$\sigma_{grad\,nl} = \sigma_{cr,max} - a_{grad}.\left(grad(\sigma_{cr})\right)^{n} < \beta_{cr} \qquad (6)$$

- σ_{ave} : Stress average volume approach

The integral approach considers the stress gradient of the stress field via an average of the stresses in a sphere of radius *r*. With this method, we can dispense with any spatial direction calculation for the calculation of the stress gradient. The parameter of the criterion to be identified is simply the radius of integration.

In order to test the criterion proposed in this paper (Eq. (3)), we used Lanning's database metal notched specimens (9). We have chosen to use this single base to guarantee the same state of preparation - machining and polishing of the notches - indeed, the Ti-6Al-4V is sensitive to these last parameters. We extracted the values of the Haigh diagrams from the author's publications. For one type of test, same geometry and same load, between 1 and 4 specimens were used per step, making it possible to obtain a fatigue limit at 10^6 cycles for each of them.

We decided to use the average of the fatigue limit, so one type of test is associated with a single fatigue limit. The characteristics of the database are given in Table 1. Three notch root radii are machined: 127 μm, 203 μm and 330 μm. From the 17 notched specimens, 9 specimens have a radius of 330 μm; 6 have a radius of 127 μm and 2 specimens have a radius of 203 μm. Most tests are conducted for load ratios of R=0.1 and R=0.5. Other specimens, made of base metal without notches, are also part of Lanning's database, there are five of them called “base metal reference”. They are tested at different load ratios between R=-1 and R=0.8.

Specimen	R	Number of test	Amplitude fatigue limit «net section» average [MPa]	ρ [µm]	D [mm]	d [mm]
lan_197_01	0,1	3	181	330	5,720	5,520
lan_230_01	0,1	2	160	330	5,720	5,310
lan_258_01	0,1	2	152	330	5,720	4,960
lan_272_01	0,1	1	123	330	5,720	4,260
lan_285_01	0,1	4	132	127	5,720	5,470
lan_286_01	0,1	2	137	203	5,720	5,210
lan_351_01	0,1	2	101	127	5,720	5,160
lan_407_01	0,1	4	93	127	5,720	4,450
lan_197_05	0,5	4	131	330	5,720	5,520
lan_230_05	0,5	3	104	330	5,720	5,310
lan_258_05	0,5	3	87	330	5,720	4,960
lan_272_05	0,5	2	78	330	5,720	4,260
lan_285_05	0,5	3	97	127	5,720	5,470
lan_286_05	0,5	2	85	203	5,720	5,210
lan_351_05	0,5	4	77	127	5,720	5,160
lan_407_05	0,5	4	64	127	5,720	4,450
lan_272_-1	-1	3	178	330	5,720	4,260
lan_100_-1	-1	2	481	-	5,700	-
lan_100_01	0,1	2	262	-	5,700	-
lan_100_05	0,5	2	176	-	5,700	-
lan_100_065	0,65	2	145	-	5,700	-
lan_100_08	0,8	2	88	-	5,700	-

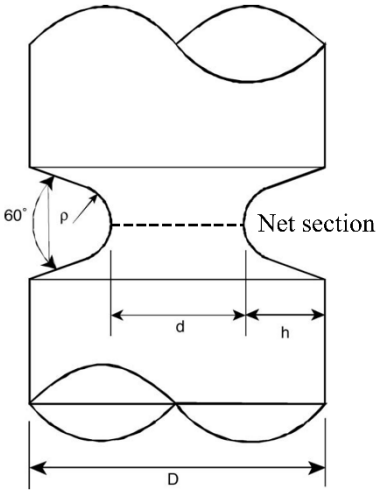

Table 1 : Lanning's notched specimens (9).

For each type of test, a finite element model is produced via the Abaqus software. The models are 2D axisymmetric using quadratic element (CAX6M). A mesh size of 50 µm was applied to the surface around the notch. The material behavior is elastic, Young modulus is equal to 110 GPa and Poisson coefficient 0.32. The simplicity of this model was intended to test criteria in a limited time while maintaining a relatively good quality of the stress field. The mesh size allows to have a 10% maximum error on the local stresses at the hotspot.

According to the information given by Lanning, the machining of the notches does not alter the fatigue properties of the material. Thus, the parameters of the Crossland criterion have no reason to be different from those of the base metal. Since notched specimens are macroscopically stressed at load ratios between R=-1 and R=0.8 the parameters of the Crossland criterion have been identified on this interval on the base metal. The method chosen consists in interpolating by a line the points of load ratio R=-1; R=0.1; R=0.5; R=0.65 and R=0.8 present in a Crossland diagram; the guiding coefficient giving α_{cr} and the ordinate at the origin giving β_{cr}. The parameters obtained are: α_{cr} = 1.494 and β_{cr} = 479 MPa and will be used for the five models tested for notched specimens ($\sigma_{cr,max}$, σ_{grad}, $\sigma_{grad\ nl}$, σ_{ave}, σ_{sd}).

The strategy that aims to identify the parameters of the non-local part on the entire database has been retained, this allows a finer comparison of the errors produced by the different criteria. For example,

with the criterion σ_{sd} the identification of the parameters r and γ is done on the entire database (17 notched specimens). They are chosen simultaneously and can be seen as a couple of parameters; one is not separable from the other. The indicator for choosing the couple is the coefficient of correlation, which is obtained for each r, by interpolating the points of the database by a line in the diagram σ_{cr} function of $sd(J_{1,max})_r$. The line has an ordinate at the origin fixed by β_{cr} and a free guiding coefficient that corresponds to parameter γ (Fig. 3a). Among the different sizes of the integration domain (from 0 µm to 500 µm) the best correlation was obtained for r = 300 µm and γ= 3.55. For the σ_{grad} criterion the a_{grad} parameter obtained is 0.06 mm. For the $\sigma_{grad\ nl}$ criterion, the parameters obtained are σ_{grad} = 44.43 mm and n = 0.18. For the σ_{ave} criterion the integration radius is 150 µm.

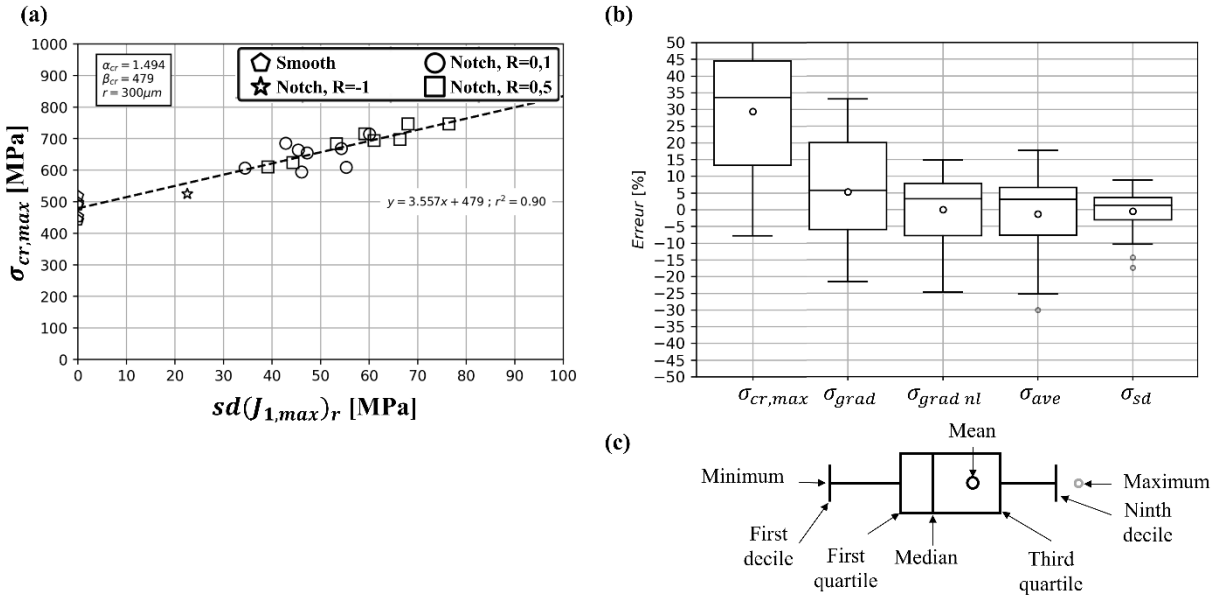

Fig. 3 : $\sigma_{cr,max}$ function of $sd(J_{1,max})_r$ for an integration radius r = 300 µm ; (b) Errors made for all five fatigue criteria ; (c) Plot box definition.

The analysis of the different approaches made it possible to evaluate the capabilities of our new criterion σ_{sd}. The capacity of each of the five criteria is evaluated by an error calculation by Eq. (7), $\sigma_{criterion}$ being one of the five used criteria performed for each type of test for the 17 specimens in the notched specimen's database and the 5 of base metal. The errors results are represented in the form of plot boxes, the characteristics of which are detailed in Fig. 3c.

$$Error[\%] = \frac{(\sigma_{criterion} - \beta_{cr}) * 100}{\beta_{cr}} \qquad (7)$$

We do not develop here the error values for each type of specimen, however the errors produced by the models can be dependent on the notch root radius or the load ratio. The local Crossland value has a load ratio dependency, while linear gradient and stress average volume approach have a notch root radius dependence. This highlights the fragility of these three approaches and questions their predictive capacity for different notches geometries. The non-linear gradient approach, however, made

it possible to make the criterion independent of geometry and load ratio. This is due to the addition of a parameter denoted *n*, which gives a non-linear weight to the gradient. Unlike other approaches, which have a single non-locality parameter to identify, this criterion has two. Thus, the use of a single parameter to capture the stress gradient seems too poor at this stage. The stress average volume approach makes it possible to overcome any gradient calculation, however, one can wonder about the physical meaning of this approach. Indeed, the maximum stress is not necessarily confused with the initiation site. The independence of the σ_{sd} criterion to the load ratio and the notch root radius highlights its predictive quality and our confidence in its ability to describe other notch geometries and load ratios. The range of the plot box of errors committed by σ_{sd} is between -10% and +10% which is the order of magnitude of the variation of the fatigue limits obtained experimentally. Comparison of the criterion with those in the literature presented in Fig. 3b shows that σ_{sd} is an interesting approach while the cost of identification through γ and *r* is just the addition of one parameter compared to other approaches using single parameter to describe gradient effect.

For each specimen, the distribution of Crossland stress present in the integration zone was analysed. The statistical series are composed on average of 120 elements and show that the distribution is not Gaussian but qualitatively symmetrical and Laplacian. The distributions morphologies are relatively close, although coming from a wide range of specimens, which is why there are inevitably differences on the distribution tails, but these have little weight on the standard deviation calculation. The four rules justifying the comparison of standard deviation are respected.

Application to defects

With the aim of defining acceptance defect size criterion, we have tested the σ_{sd} criterion in the case of porosity in welded junction. The criterion allowed us to evaluate the capacity in the case of interaction between two defects (defect/defect interaction), interaction between the defect and the surface of the specimen (defect/surface interaction) and for the defect size effect. Different types of defects were studied, allowing us to explore the key hypothesis of the identification strategy which is the independence of non-locality parameters to the type of concentrator. For our study we relied on Ti-6Al-4V butt joint specimens welded by electron beam. Within the joint, we find natural gas porosities related to the welding process. We also machined artificial defects on the specimen's sides to study the defect size effect and the interactions between two defects (Fig. 4a). All four defect types are presented in the following. All artificial defects are machined exactly in the same location in the welded junction (Fig. 4a) in order to have the same microstructure surrounding the defect. Of course natural gas pores can be located in different position through the welded junction but it was relatively closed to the location of artificial defects.

Artificial milled defect, fast speed

The first type of defect was achieved with a rapid machining mill at a rotation speed of 6720 rpm and a travel speed of 0.05 mm/s. It was chosen because it allows to create a spherical morphology of the deep part of the defect. The fast speed allows, in theory, to reduce as much as possible the peculiarities generated by machining (surface finish, microstructure ...). To remove the residual stresses generated by the manufacturing process, a common vacuum heat treatment of 680°C/2h was applied (12).

Isolated defects machined have been machined, their size in $\sqrt{area}$ (13) varies from 134 μm to 1732 μm. Other defects were machined to generate defect interaction, the four types of interactions performed are shown in Fig. 5b. The nomenclature chosen is as follows: "d1:d2", d1 and d2 are the mill diameters of the two artificial defects created, of respective depths 3/4d1 and 3/4d2 in order to have a defect size in $\sqrt{area}$ independent of the projection axis. The size ratios (d2/d1) are multiple: 1, 1/2 and 1/5 (Fig. 4b).

Natural porosities

Fourteen natural porosities have been studied, they come from the electron beam welding process and have spherical morphologies of gaseous type. Although the origin of the rupture comes from a porosity, the neighbourhood may be different. Four families of models were considered: Null Ligament (NL), Ligament (L), Without Ligament (WL) and Cluster (C) (Fig. 4c). The ligament is the minimum distance between the porosity and the surface or between two porosities. A cluster is defined as two defects that are close to each other. Except WL family, all of these configurations are considered as defect/surface interaction. The "Null ligament" family, rated NL, owns 50% of the results. It is composed of specimens whose ligament size could not be correctly quantified by the fracture surface, because too small. We made the choice, for this family to impose a ligament of 1 μm on the numerical model. The second modelling family is "Ligament", denoted L, it counts 35% of the results. It is composed of specimens whose ligament size could be correctly quantified on the fracture surface; an example is given in Fig. 4c. The minimum size of a ligament is 11 μm, which is much larger than those of the Null Ligament family. The last two families are each composed of a specimen, they correspond to the families: "Without ligament" (WL): these porosities do not have a ligament and their formation is linked to the cutting of the specimens and "Cluster" (C): this specimen has several porosities forming a cluster. Their fracture surface are presented in Fig. 4c.

Artificial drilled defect, slow and fast speed

The last types of defects were machined with drill tools. Two machining speeds were applied, a fast one as previously for the "artificial milled" defect type, and a slow one with a travel speed of 0.001 mm/s and a rotational speed of 4900 rpm. In the same way as for defects made by milling a heat treatment of 680°C/2h was applied. The $\sqrt{area}$ of these isolated defects ranges from 176 μm to 1233 μm. The configurations of these defect types all correspond to the defect size effect. The machining speed impacts the morphology of the defect, as shown in Fig. 4d and Fig. 4e. Indeed, for a fast speed, the mark left by the drill head is prominent, while for the slow speed, it is more rounded. This rounded shape is probably due to the micro-vibrations characteristic of slow machining speeds, which give amplitudes to the movements of the drill. The second change caused by speed is the surface integrity. Indeed, scales are found on the defects for both speeds, but are in greater number and smaller size for the slow configuration (Fig. 4d, Fig. 4e). They are also probably due to micro-vibrations.

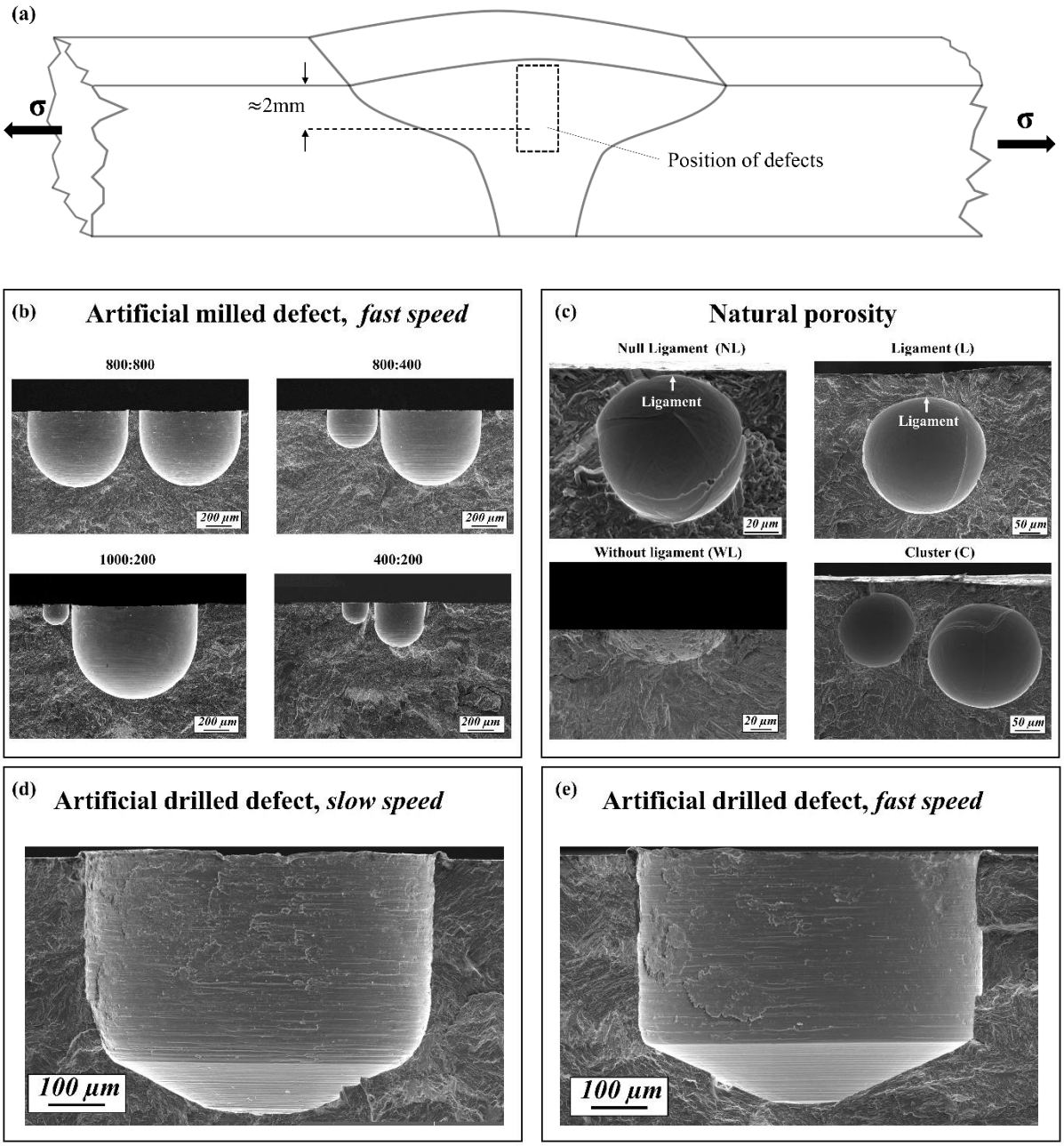

Fig. 4: (a) Artificial defects localization on the side of flat tension fatigue welded specimen; (b)(c)(d) Fracture surface for 4 types of defects.

The step method is the heart of our testing strategy (14), for steps at 10^6 and for increases between each step of 5% to 10%, i.e. an increase in steps of 10 MPa on the stresses amplitude. The fatigue limit is then deduced with the breaking step and the one preceding it via Eq. (8) with σ_n the stress applied to the breaking step, σ_{n-1} the stress applied to the last non-rupture step and N the number of cycles to failure.

$$\sigma_a = \frac{N}{10^6} * (\sigma_n - \sigma_{n-1}) + \sigma_{n-1} \quad (8)$$

The $\sqrt{area}$ size covered by defects in the "Milled" database varies from 134 μm to 1732 μm for the base "Drilled, slow" varies from 176 μm to 1233 μm. The size effect for the defects achieved by milling is presented in Fig. 5, we find that between a size of 150 microns and 1500 microns, the decrease is 60 MPa. From a size of about 1000 μm there is a saturation of the size effect. For defects made with a drill at slow speed, the observation previously made is similar. In addition, the trend of the milled defects curve is very close to that of the defects made by drill, the latter is just shifted down by 60 MPa. For defects made by mill and drill, according to the analysis of the fracture surfaces, the preferred area for the fatigue cracks initiation seems to be the cylindrical part of the defect, which is consistent in view of the overstress generated by the cylindrical part. Thus, what differentiates these two defects would be more their type than the morphology of the cylinder. The 60 MPa difference between mill/drill defects can be explained only by the type of defects (surface finish, residual stresses, microstructure). Another series of fatigue test was conducted on samples containing semi spherical surface electro discharge defect in the same location. The results were not analysed into details compared to the other defects because it is well known that EDM machining is not recommended for Ti-6Al-4V. Nevertheless, it is another confirmation that the type of defect plays an important role in Ti-6Al-4V and that the unique ‘size’ parameter is not always relevant to characterise the impact on the fatigue limit. Regarding these impact on the fatigue limit, the type of defect is therefore very important for Ti-6Al-4V. This observation is consistent with the work of Léopold (15) and Simon (16). The Kitagawa diagram also shows the point corresponding to drill machining at fast speed, which is lowered compared to those at slow speed. This is due to the same reasons as before to the type of defect. For comparison purposes, the points of the natural porosities are also shown on the diagram. Their equivalent size $\sqrt{area}$ was calculated using the rules presented in Fig. 5b and Fig. 5c. This methodology quantifies the effect of the interacting defect(s) through an equivalent size. It considers the surface of the defect combined with that of the ligament.

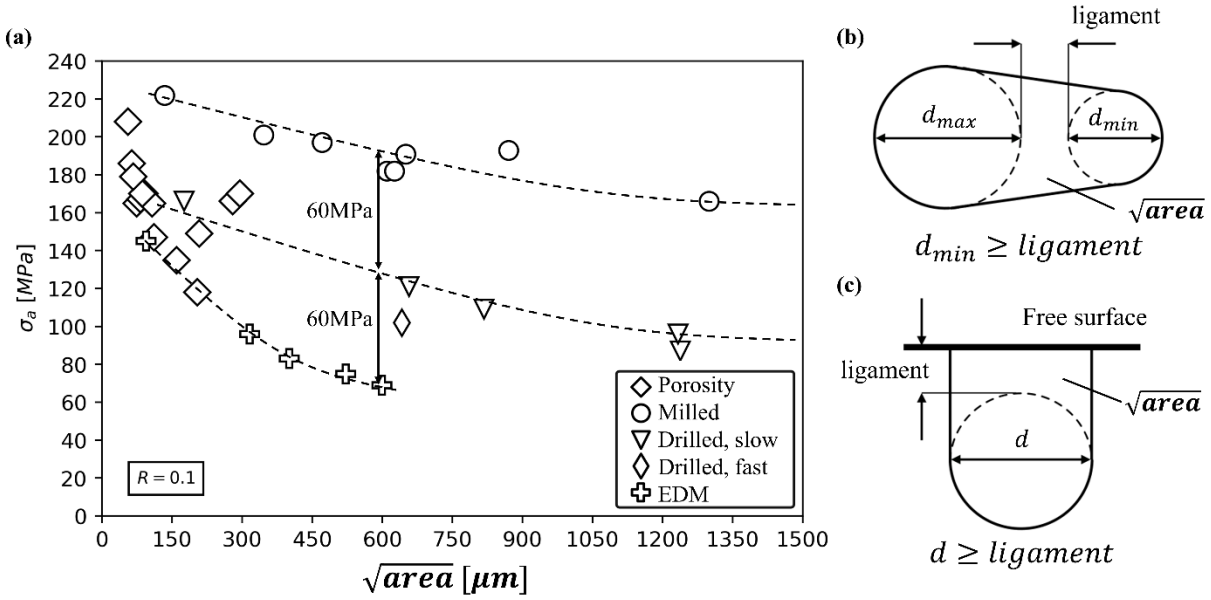

Fig. 5: (a) Kitagawa diagram: natural porosities and artificial defects. Evaluation of the effective defect size for natural porosities: (b) Defect/defect interaction (c) Defect/surface interaction.

The numerical analysis of Murakami and Nemat-Nasser shows that the interaction distance, the distance from which two defects interact, is one time the diameter of the smallest defect (13). In our study we consider that there is no more interaction if the fatigue limit is greater than or equal to 180 MPa, this value corresponds to the limit of the isolated defect size. Regardless of the type of interaction, the experimental interaction distance is less than once the diameter of the smallest defect, for example, for 800:800, the interaction distance is 0.2xdmin and for 800:400, it is 0.7xdmin. We can explain this finding in several ways. The numerical study of Murakami is carried out using local values of stresses, via the indicator $K_{I,\,max}$, but no consideration of the stress gradient is performed. However, for a defect present in Ti-6Al-4V, a local value is often conservative against fatigue, the interaction distance is therefore overestimated. The second explanation may be as follow: the numerical study is carried out with cracks and not defects. Thus, if the defect does not behave like a crack against fatigue, the study is unreliable. Moreover, if the defect is less sensitive to fatigue than the crack, then the interaction distance is overestimated. The use of the largest defect diameter instead of the smallest minimizes the interval taken by the interaction distances (Fig. 6a). Indeed, we found that the interaction distance is between 0.2 and 0.35 against 0.2 and 0.7 with the use of small diameter. Thus, the expected distance between two porosities must be determined in relation to the largest porosity and not the smallest. These interaction distance values between 0.20xdmax and 0.35xdmax highlight that it takes a very small ligament before there is an interaction between the two defects (Eq. (9)).

$$0.20xdmax \leq interaction\ distance\ values \leq 0.35xdmax \qquad (9)$$

This supports Åman's finding for materials with high hardness (17). This author notes that the interaction distance depends on the hardness of the material: the higher it is, the more the interaction distance is reduced.

Fig. 6a shows that the fatigue limit decreases qualitatively linearly as a function of the ligament size (ligament/max diameter). The diminution attributed to the presence of the ligament is very pronounced, for example for the smallest ligament, it can reach a reduction of 2.25 compared to the isolated defect. To consider this type of interaction, measurements of equivalent sizes according to Murakami's definition of interaction can be made, this one has been presented in Fig. 6b. The method consists in considering the area of the two defects and that of the area between them when the ligament is smaller than the defect. To evaluate the capability of this method, the equivalent size of each interacting defect has been obtained and plotted in the Kitagawa diagram in Fig. 6b. A reference named "without interaction" is also placed, these points correspond to the same type of defect as those in interaction milling in fast machining. In this diagram the '800 µm' isolated defect corresponds to the diameter of the defect and according to the depth equal to ¾ of the diameter the $\sqrt{area}$ parameter is 641 µm for this defect. The Kitagawa diagram in Fig. 6b clearly shows that the equivalent size measure has no predictive ability in the case of Ti-6Al-4V with interacting defects, indeed, if the measurement would be appropriate, then all points would follow the trend of the curve without interaction, but this is not the case. The measurement of equivalent size is therefore questioned, but it goes further, it reconsiders the approach proposed by Murakami and Endo in 1983, for the welded Ti-6Al-4V whose fundamental equation is Eq. (10)(18). These authors had already pointed out the limitations of their study by conclusion 4 of their article: "*When the root radius ρ at the fracture origin of a defect is greater than the critical value ρ_0, the Eq.* (10)*, are not applicable. This is because the equations hold only for cases where the fatigue limit is determined by the condition of non-propagation of cracks emanating from defects. The fatigue strength in other cases should be estimated considering stress concentration and stress gradient"* (18). However, the absence of non-propagating cracks is suspected in Ti-6Al-4V and in that carried out by Åman on the presence of defects (17). It is therefore supposed that there are no non-propagation cracks in Ti-6Al-4V. Thus, in our case, the welded Ti-6Al-4V does not meet the criteria for applying the equation, so Murakami's approach is not really suitable.

$$\sigma_w^n \sqrt{area} = C \qquad (10)$$

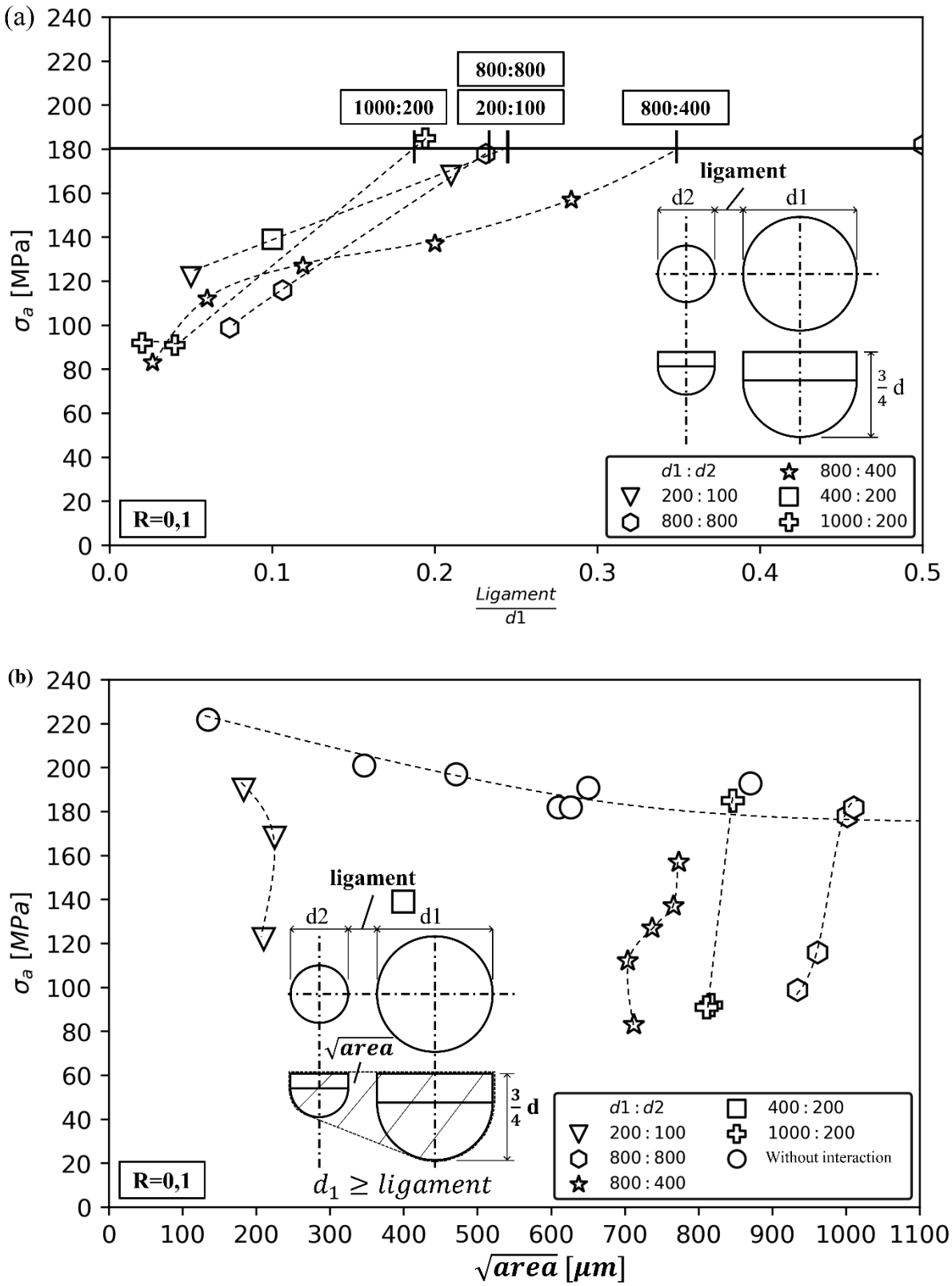

Fig. 6 : (a) Fatigue limit amplitude depending on ligament size (ligament/d1); (b) Kitagawa diagram: isolated defects and interacting defects.

In order to apply the σ_{sd} criterion, we need a finite element model to obtain the stress fields around defects. In order to simplify the study the entire specimen was not modelled. We have chosen to place the defects causing the rupture in a rectangular volume. The single axis of symmetry of the rectangle has been exploited to reduce the size of the model, it corresponds to the plane of normal x, passing to the centre of defects in Fig. 7. The dimensions of the rectangle must make it possible to translate an "infinite medium" around the defect, i.e. there is no influence of the volume size on the stress field close to the defect. Therefore, following the y-axis, the size of the model is 5d; and along the x and z axes, by 2.5d. The parameter *d* is the effective diameter of the defect, as a reminder, it corresponds to the diameter of the sphere that includes the defects. The volume is meshed as a quadratic triangle element C3D10 in Abaqus. To obtain a good quality stress field while reducing the model size, three mesh areas were made, they are shown in Fig. 7. The first area corresponds to the ligament. For interacting defects, the mesh size chosen is 5 µm, or about 4 elements in the thickness for the smallest ligaments. For defect interaction with the surface, the ligament size can reach 1 µm, which is why for these cases the mesh size in the ligament area is 0.5 µm, which is 2 elements in the thinnest area. The second area is a rectangle including the defects, the chosen mesh size is 1/20 of the diameter of the smallest of the defects. This mesh rule has a good description while having a small number of elements. Finally, the third area is composed of a gradient of mesh sizes that reaches a size of about 0.5d at the ends. The plastic behavior used is a non-linear kinematic hardening proposed by Chaboche (19) of parameters E = 110GPa, ν = 0.32, σ_0 = 650 MPa, C_0 = 536GPa and γ_0 = 1500. Those parameters are extracted from a study of the literature (20).

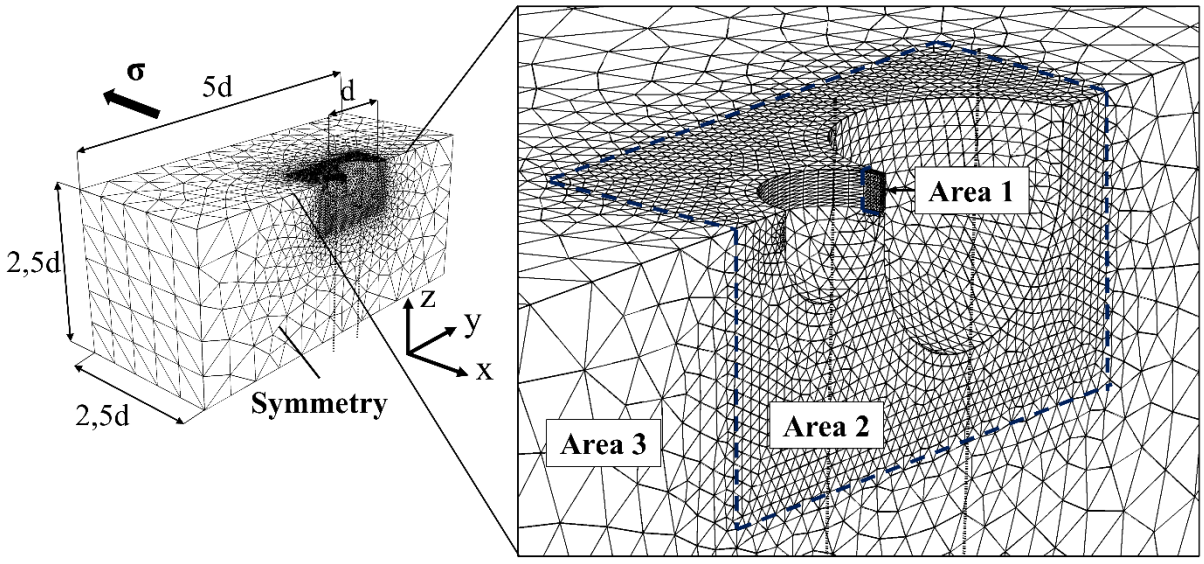

Fig. 7 : Modelling rules.

The database with the most varied morphologies is the "Artificial milled defect, fast speed" type, in fact, it is composed of 22 models, 13 of which have interacting defects. The parameters of non-locality *r* and γ will therefore be identified on this basis, they will then be used for the other types of defects. For criterion σ_{sd}, the quantity $sd(J_{1,\,max})_r$ is obtained for the integration radii of 30 μm, 40 μm, 50 μm and 100 μm ; for each model. For each radius, a diagram: $\sigma_{cr,max}$ function of $sd(J_{1,max})_r$ is plotted, and a linear interpolation is performed. The best correlation coefficient is obtained for a radius of 50 μm (Fig. 8a). The β_{cr} parameter is re-evaluated for each defect type (Table 2). For the local value, the parameter β_{cr} is the average of the local stresses acquired over all models.

Defect type	$\sigma_{cr,max}$	σ_{sd}		
	β_{cr} [MPa]	β_{cr} [MPa]	*r* [μm]	γ [ ]
Artificial milled defect, *fast speed*	773	687	50	4,43
Natural porosity	623	494	50	4,43
Artificial drilled defect, *slow speed*	513	445	50	4,43
Artificial drilled defect, *fast speed*	446	397	50	4,43

Table 2 : σ_{cr} and σ_{sd} identification parameters.

Artificial milled defects

In order to use the fatigue criterion σ_{sd}, the use of the standard deviation must first be justified. We observe two types of stress distributions in the integration domain: symmetric and non-symmetric. Thus, the comparison of the standard deviation value is not fully justified, but this does not appear to be detrimental in relation to the errors produced by the criterion σ_{sd} (Fig. 8b). Indeed, the interval of the error committed by the local value is 49% while the criterion σ_{sd} leads to 29%, i.e. a reduction of the domain of 20%. Thus, to capture the defect size effect and the interaction effect between two defects, the stress gradient of the stress field must be considered.

Defect/defect interaction

The stress heterogeneity in the integration sphere reflected using the standard deviation depends on defect size ratio (Fig. 8a). The greater the size ratio between two defects, the more fundamental it is to capture the stress gradient in a fatigue criterion. Thus, for the ratio of 1, regardless of the size of the ligament, the stress gradient does not need to be considered; for the 1/2 ratio, the stress gradient must be taken into account for small ligament values; and for ratios greater than 1/2 stress gradient must be considered for any ligament size.

Defect size effect

Nine isolated defects, with diameters between 200 μm and 2000 μm, were studied. The fatigue limits are shown in Fig. 5a. For these same points, the diagram σ_{cr} function of $sd(J_{1,max})_r$ is plotted in Fig. 8a. The latter shows that the parameter $sd(J_{1,max})_r$ is relatively high for small diameters and reaches a saturation from the diameter of 600 μm. Thus, for small defect sizes, the stress gradient needs to be considered. The parameter set used in the σ_{sd} criterion is unique to deal with problems of defect size

effect and defect/defect interaction. However, this set of parameters obtains small errors independent of the effect processed. This suggests that whatever the problem - defect size effect or defect/defect interaction - the stress gradient is of the 'same nature'.

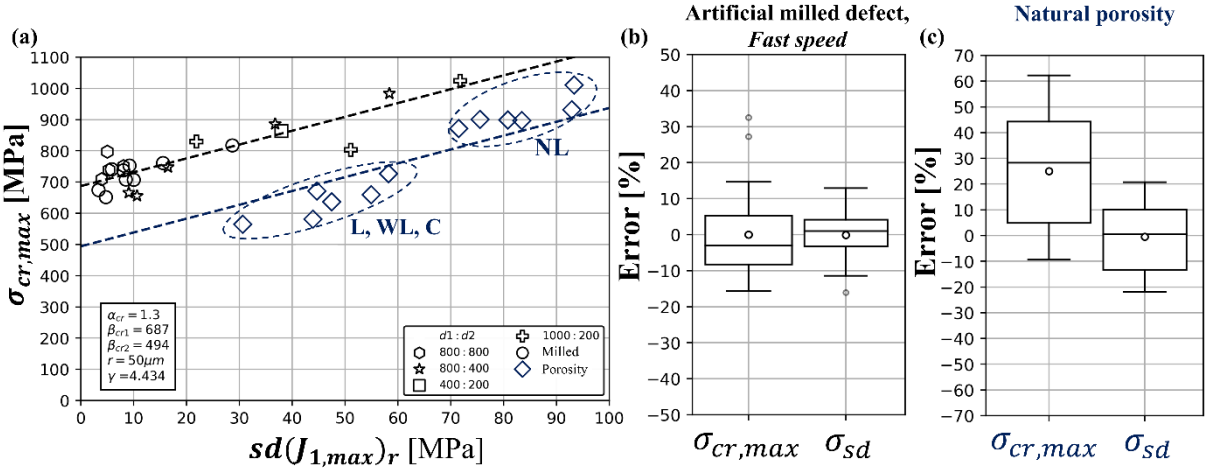

Fig. 8 : (a) $\sigma_{cr,max}$ function of $sd(J_{1,max})_r$ for an integration radius r = 50 µm, the types: « Artificial milled defect, fast speed » and « Natural porosity » are displayed; Errors made by fatigue criteria: (b) For the « Artificial milled defect, fast speed » (c) For the « Natural porosity ».

Natural porosities

For natural porosities, the range of the error using the local value is 71%. This important value highlights that a local value is too poor to describe the natural porosities fatigue limit. The use of criterion σ_{sd} reduces this interval by 28%, with an error of 43% (Fig. 8c). Thus, to capture the interaction effect between a defect and the surface, the stress gradient of the stress field must be considered. It should be noted that the use of the standard deviation present in σ_{sd} is fully justified regarding the stress's distribution in the integration volume. We have shown that there are two distinct groups of local value errors for natural porosities, composed respectively of the L, WL and C families; and the NL family. In view of the reduction in the error interval due to the use of σ_{sd}, the use of this criterion made it possible to bring the two groups together. This means that the origin of these two groups comes mainly from the stress gradient. However, we see in Fig. 8a, that the group composed of the families L, WL and C is under the interpolation curve, and the group composed of the family NL is above the curve. Thus, the non-local fatigue criterion certainly allows a reunification, but this is only partial, the sign of the error using the criterion σ_{sd} depends on the family considered. This limitation could have two explanations: the fatigue criterion (writing and identification) or finite element modelling (material behavior and geometry), but we are not able to define the preferred interpretation path.

The element that increased the predictive ability of fatigue limit is related to the use of $sd(J_{1,max})_r$. It is obtained on the series of constraints $J_{1,max}$ present in the integration volume. A defect is composed of a mechanically loaded area and other unloaded areas, and since the defect size is relatively close to the integration domain size, part of the integration stress area is mechanically unloaded. An example is given in Fig. 9, it highlights that a significant part of the stress of the series is lightly loaded. Thus, it

seems that it is the mechanically unloaded areas, present in $sd(J_{1,max})_r$, which have increased the ability to predict fatigue limit. This observation is similar to that made on the notched specimens which showed that a significant part of the stress of the integration zone were lightly loaded. Yet it is with these unloaded areas that the criterion manages to describe finely the fatigue resistance in the presence of geometric singularities. These observations make it possible to answer to the fundamental question: "*Do poorly mechanically loaded areas participate in the fatigue mechanism?*". It seems that "*yes*", this track of interpretation will be developed in the rest of this paper.

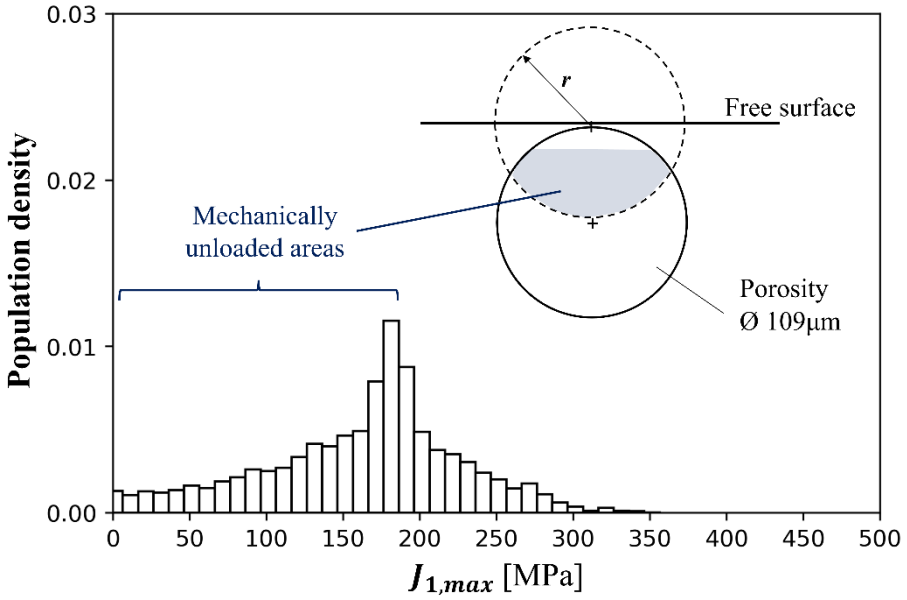

Fig. 9 : Distribution of $J_{1,max}$ over the integration domain for the calculation of the standard deviation for a porosity near the surface.

Artificial drilled defects

The defect morphology is composed of a cylindrical upper part and a conical lower part, more or less depending on the drilling speed, examples in slow and fast speed are given respectively in Fig. 4d and Fig. 4e. The study of five models allowed us to find that, regardless of the machining speed and the diameter of the drill, the value of the maximum Crossland stress is located on the cylindrical part of the defect (Fig. 10b). Thus, the geometry of the lower part (conical or spherical) of the defect would have less impact on the fatigue limit. This finding is supported by the previous finding that the preferred area for cracks initiation appears to be the cylindrical part of the defect. Thus, the differences in fatigue limit found on the Kitagawa diagram for the three types of defects: milled, drilled fast and slow speed (Fig. 5a) are attributable to the cylindrical part morphology and the type of defect (residual stresses, microstructure and surface finish).

We have shown that to describe the milled defects size effect, the stress gradient had to be considered. It is the same for the drilled defects size effect, in fact, a local value of stress obtains an error interval of 51% against 24% with the σ_{sd} criterion; the decrease in the interval is therefore 27% (Fig. 10c). It should be noted that the use of the standard deviation present in σ_{sd} is justified, regarding the stress distribution in the integration volume. The first objective of this part is to compare the identification strategy whose main hypothesis is the independence of the non-locality parameters of the criterion to the type of concentrator. The non-locality parameters of criterion σ_{sd} are *r* and γ, where γ is the guiding coefficient of the lines present in the diagram σ_{cr} function of $sd(J_{1,max})_r$, in Fig. 10a. For the "Artificial drilled defect, slow speed" type, blue in this figure, the four points qualitatively follow the line of γ direction coefficient and tangent originally 445 MPa. Thus, although *r* and γ are obtained for milled defects, they are suitable for "Artificial drilled defect, slow speed" so the previous assumption is verified for this case. The fatigue criterion σ_{sd} captures the morphology effect and the effect of the type of defect. The β_{cr} parameter has more particularly the information of the type of defect, i.e. the residual stresses, the microstructure and local roughness generated by the machining process. However, β_{cr} is different for each type of defect. This allows us to answer another question: "*Why is the fatigue sensitivity of milled and drilled defects different? »*. The answer is related to the defect type.

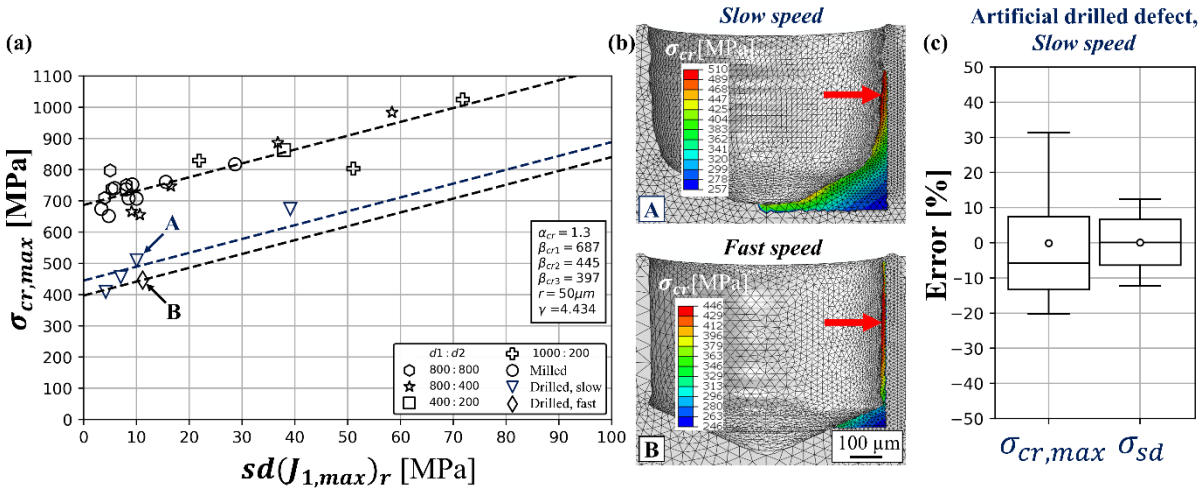

Fig. 10 : (a) $\sigma_{cr,max}$ versus $sd(J_{1,max})_r$ for an integration radius r = 50 µm, the types: « Artificial milled defect, fast speed », « Artificial drilled defect, slow speed » and « Artificial drilled defect, fast speed » are displayed; (b) Crossland stress field for slow and fast machining speeds; (c) Errors in fatigue criteria for the « Artificial drilled defect, slow speed ».

The main hypothesis of the identification strategy is the independence of the non-locality parameters to the type of concentrator. This means that for the four types of defects there is a single set of non-locality parameters. We will discuss this hypothesis, which has been tested here by: defect types, interactions, and the associated FE models. Indeed, we have shown that the differences in fatigue limit between the four defects were mainly related to their type: residual stresses, microstructure and roughness surface generated by the machining process. However, the information of the type of defect is mainly contained in the parameter β_{cr}. The values taken by β_{cr} vary almost double, so the defect type has been greatly exacerbated. In addition to the type, there are three interactions: defect/defect, defect/surface and defect size effect. In total, the number of cases treated is 41. Since the errors generated by criterion σ_{sd} are reasonable, with the assumption of the independence of the non-locality parameters to the type of concentrator, this assumption seems quite valid. An attempt to explain this independence is one of the objective of the following discussion.

Discussion

The stress heterogeneity indicator within the integration domain was the standard deviation. It turns out that integrating the stress variation into a criterion allows a good predictive capacity. This observation being relatively empirical, we seek to better understand it. Susmel in 2008 introduced the idea of "structural volume" to explain why critical distance theory is effective. To our knowledge, this is the richest explanation attempt in the literature because it explains why methods of describing fatigue limit have a predictive capacity although based on totally different concepts. According to him: "*All the physical processes resulting in the formation of fatigue cracks are confined within a finite volume. The size of this volume is assumed to be constant (but different for different materials) and it depends on neither the geometrical feature nor the degree of multiaxiality of the stress field damaging the fatigue process zone* " (21). The properties proposed by the author are shown in Table 3. The idea of structural volume and its four properties proposed by Susmel are consistent with our observations

of the model. Indeed, for the same type of concentrator, we try to obtain the fatigue strength for several geometries, but the integration volume and the weight given to this volume are unchanged although the geometries are different. Thus, the two properties of the structural volume: "finite volume" and "size independent of geometry", seem quite plausible to us. In this study two distinct materials were studied: Ti-6Al-4V base metal and welded Ti-6Al-4V. Base metal Ti-6Al-4V was used for notched specimens and welded Ti-6Al-4V for defect specimens. The optimal integration volume between the two materials is different, this must be qualified in view of the small number of materials studied. Additional studies would be required to confirm this analysis. Thus, the property of structural volume: "material-dependent size", seems to us quite plausible. The last property proposed by the author: "size independent of the stress field" means that the structural volume can have mechanically overloaded but also unloaded areas. Depending on the acuity of the geometry, the stress present in the structural volume will be even more dispersed. This property of the structural volume proposed by Susmel explains the existence of mechanically unloaded areas in integration zones of optimal size. Indeed, we have shown, for notched specimens and for those with natural porosities, that the importance of mechanically unloaded areas was not insignificant. However, it is thanks to these unloaded areas that the criterion manages to describe accurately the fatigue resistance in presence of geometric singularities.

Properties offered by Susmel (21)	**Additional properties proposed in this study**
Finite volume	Volume close to a sphere
Stress field independent size	
Geometry independent size	Concentrator type independent size
Material dependent size	

Table 3 : Structural volume properties.

The four properties proposed by Susmel to the structural volume are consistent with our observations and make it possible to give plausible explanations on fundamental questions. Thus, we are confident about the notion of structural volume and its properties. We will now carry out the opposite process: starting from the observations of the model to deduce new properties of the structural volume. The first of the properties we want to study is the morphology of the structural volume. In this study, the integration volume is a sphere, but this morphology has made it possible to treat very different geometries. Thus, it is likely that the structural volume is qualitatively of this morphology. In addition to the model, an identification strategy is proposed. Its main hypothesis is the independence of non-locality parameters to the type of concentrator, parameters that define the size of the integration zone and the weight given to the variations in the stresses present in this zone. This strategy has been extensively tested for the different types of defects. However, if the structural volume is insensitive to the type of concentrator, then the following totally empirical observation would be explained: the size of the integration domain and its weight are independent of the type of concentrator.

The structural volume has properties consistent with those of the model and explains aspects of the criterion as yet only observed (mechanically unloaded areas). The criterion seems justified because it makes it possible to characterize the structural volume, in particular its morphology and its relationship of independence to the type of concentrator. Our criterion demonstrates a good ability to

understand the properties of the structural volume, to improve its capacities it is therefore necessary to continue to be in harmony with the characteristics of the structural volume.

We believe that improving the predictive capacity of models requires a good appreciation of the structural volume. Thus, it seems quite appropriate to continue to use a finite integration zone, to keep the fundamental idea of finite volume. The integration zone morphology can remain spherical, since it seems that the shape of the structural volume has this characteristic. Since the structural volume is of a size independent of the stress fields, mechanically unloaded areas are likely to be found. Although they can be lightly loaded, we think that they occur in the fatigue mechanisms in the presence of a stress concentrator, these discharged areas must be integrated into the calculation of stress gradient.

Conclusion

Fatigue data (Tension, High Cycle Fatigue, 10^6 cycles) related to titanium Ti-6Al-4V were analysed to understand the stress gradient effect associated with stress concentrators. The cases covered are macroscopic notches and micro-defects (defect size effect, defect/defect interaction, surface/defect interaction). The conclusions of this work are as follows:

- We have shown that the type of concentrator is of prime order for Ti-6Al-4V fatigue limit: for the same geometry and size, the type of defect strongly changes the fatigue limit.
- The interaction distance, the distance from which two defects interact, is small: 0.20-0.35 times the biggest defect and the ligament effect is very pronounced. To deal with interaction, the equivalent defect size $\sqrt{area}$ approach proposed by Murakami is very conservative.
- The stress gradient has been quantified through the standard deviation of the variation of $J_{1,max}$ stresses over the integration domain, it is denoted $sd(J_{1,max})_r$. The criterion σ_{sd} shows a good predictive ability for: notches, defect size effect, defect/defect interaction, defect/surface interaction. An explanation of the predictive capacity of the criterion (writing + identification) has been formulated, involving the idea of structural volume. We believe that the predictive capacity of the model requires a good appreciation of this volume.

$$\sigma_{sd} = \sigma_{cr,max} - \gamma . sd(J_{1,max})_r \leq \beta_{cr}$$

- We assume that the parameters r and γ are independent of the type of concentrator and therefore applicable to all types of concentrators. The β_{cr} parameter is identified for each type of concentrator, so it has much of the information related to surface integrity of the concentrator. This strategy has been tested with relevance in this study.

References

1. Taylor D. Geometrical effects in fatigue: a unifying theoretical model. International Journal of Fatigue. mai 1999;21(5):413‑20.

2. Papadopoulos IV, Panoskaltsis VP. Invariant formulation of a gradient dependent multiaxial high-cycle fatigue criterion. Engineering Fracture Mechanics. nov 1996;55(4):513‑28.

3. Nadot Y, Billaudeau T. Multiaxial fatigue limit criterion for defective materials. Engineering Fracture Mechanics. janv 2006;73(1):112‑33.

4. Sonsino CM, Kaufmann H, Grubišić V. Transferability of Material Data for the Example of a Randomly Loaded Forged Truck Stub Axle. In 1997. p. 970708. Disponible sur: https://www.sae.org/content/970708/

5. El May M, Saintier N, Palin-Luc T, Devos O. Non-local high cycle fatigue strength criterion for metallic materials with corrosion defects. Fatigue Fract Engng Mater Struct. sept 2015;38(9):1017‑25.

6. Pessard E, Bellett D, Morel F, Koutiri I. A mechanistic approach to the Kitagawa–Takahashi diagram using a multiaxial probabilistic framework. Engineering Fracture Mechanics. sept 2013;109:89‑104.

7. Vincent M. Interaction entre défaut de surface et taille de grain en fatigue à grand nombre de cycles : approche expérimentale et numérique sur un fer pur Armco, PhD, ISAE-ENSMA, 2018.

8. Heyraud H. Caractérisation expérimentale et modélisation du comportement en fatigue à grand nombre de cycles des structures soudées : application aux engins de manutention, PhD, ENSAM, 2021.

9. Lanning D, Nicholas T, Palazotto A. The effect of notch geometry on critical distance high cycle fatigue predictions. International Journal of Fatigue. oct 2005;27(10‑12):1623‑7.

10. Crossland B. Effect of large hydrostatic pressures on the torsional fatigue strength of an alloy steel. In London; 1956. p. 138‑49. (The third int. conf. of fatigue of metals).

11. Dal Cero Coelho F. Maîtrise de la tenue en fatigue des cordons de soudure, PhD, ISAE-ENSMA, 2015.

12. Fomin F. On the fatigue behaviour and modelling of fatigue life for laser-welded Ti-6Al-4V, PhD, Technischen Universität Hamburg, 2019.

13. Murakami Y. Metal Fatigue: Effects of Small Defects and Nonmetallic Inclusions. Elsevier; 2002.

14. Maxwell DC, Nicholas T. A rapid method for generation of a Haigh diagram for high cycle fatigue. 1998.

15. Léopold G. Influence des défauts de fonderie sur la tenue en fatigue d'un alliage de titane moule, PhD, ISAE-ENSMA, 2011.

16. Simon J. Influence de micro-entailles sur le comportement en fatigue à grand nombre de cycles d'un alliage de TA6V : Comparaison avec le fretting-fatigue, PhD, ISAE-ENSMA, 2018.

17. Åman M, Wada K, Matsunaga H, Remes H, Marquis G. The influence of interacting small defects on the fatigue limits of a pure iron and a bearing steel. International Journal of Fatigue. juin 2020;135:105560.

18. Murakami Y, Endo M. Quantitative evaluation of fatigue strength of metals containing various small defects or cracks. Engineering Fracture Mechanics. janv 1983;17(1):1‑15.

19. Lemaître J, Chaboche JL. Mechanics of solid materials. Cambridge: Cambridge University Press; 1990. 556 p.

20. Lacourt L. Étude numérique de la nocivité des défauts dans les soudures, PhD, MINES ParisTech, 2020.

21. Susmel L. The theory of critical distances: a review of its applications in fatigue. Engineering Fracture Mechanics. mai 2008;75(7):1706‑24.